scientific reports

Check for updates

OPEN

Fit analysis of 3D-printed versus thermoformed clear aligners for labial tooth movement using micro-CT: an in vitro study

Sun Young Lim[1], Sung-Hwan Choi[2], Hyung-Seog Yu[2], Sun-Hyung Park[3], Jae-Sung Kwon[4], Su-Jung Kim[5], Jing Liu[2] & Jung-Yul Cha[2,6]✉

This study examined the fit of 3D-printed and thermoformed clear aligners (CAs) on activated tooth models using micro-computed tomography (micro-CT). Three evaluation models were prepared: a passive model (P0.0) and two activated models (A0.3 and A0.5, where the upper right central incisor was labially displaced by 0.3 and 0.5 mm, respectively). Three CA material groups were tested: 3D-printed CAs made from TC-85 resin (3DP), thermoformed multi-layer CAs with a copolyester–elastomer combination (TM), and thermoformed single-layer CAs made of polyethylene terephthalate glycol (TS). CAs (n = 10) were fitted to corresponding models and scanned using micro-CT. Gap widths were measured at various tooth positions and measurement points in sagittal sections on all sides under passive and active states. Nonparametric analyses (Kruskal–Wallis tests with Bonferroni-corrected Mann–Whitney U post hoc comparisons) were performed with α = 0.05. The 3DP group exhibited significantly greater overall gap widths than the thermoformed groups ($p < 0.001$), with no significant effect of activation level ($p = 0.350$). In contrast, both the TM and TS groups showed significant increases in gap width with increasing activation ($p < 0.001$). Fit patterns differed by tooth position and measurement point, particularly in activated models, demonstrating distinct material-dependent adaptation behaviors.

Keywords Activated tooth model, 3D-printed clear aligner, Thermoformed clear aligner, Micro-CT, fit, Gap width

Clear aligner (CA) therapy has gained widespread popularity in recent years owing to its aesthetic benefits, removability, and minimal impact on daily life[1]. These advantages have driven the use of CAs across all age groups, including children and adolescents[2,3]. With growing demand, various CA materials have been developed, and their clinical performance is expected to improve as mechanical properties advance[4]. Thermoplastic materials used for CAs are classified into single-layer and multi-layer types[5]. Common single-layer materials include polyethylene terephthalate glycol (PETG), thermoplastic polyurethanes (TPU), polycarbonate, polypropylene and copolyester[6–9]. Although widely used, most single-layer materials exceed their yield strength when deformed beyond 10–15%, making recovery of the original shape difficult[10]. To address these limitations, multi-layer hybrid materials were introduced, combining a rigid outer shell with a more elastic inner core. These designs provide a lower modulus of elasticity, enabling easier insertion and removal, reduced patient discomfort, and more continuous force delivery with less stress decay[11].

With advances in computer-aided design and manufacturing (CAD/CAM) technology, 3D printing has become a novel method for producing CAs, eliminating thermoforming[12]. Several resin-based materials with favorable mechanical and biocompatible properties have been developed for 3D-printed aligners, and ongoing efforts aim to integrate them into clinical practice. In a systematic review, Boo et al. reported that most 3D-printed aligners remain within the clinically acceptable accuracy threshold of 0.25 mm[13]. Notable materials discussed

[1]Department of Orthodontics, Yonsei University College of Dentistry, Seoul, Korea. [2]Department of Orthodontics, Institute of Craniofacial Deformity, Yonsei University College of Dentistry, 50-1 Yonsei-ro, Seodaemun-gu, Seoul 03722, Korea. [3]Department of Biostatistics, Korea University, Seoul, Korea. [4]Department and Research Institute of Dental Biomaterials and Bioengineering, Yonsei University College of Dentistry, Seoul, Korea. [5]Department of Orthodontics, Kyung Hee University School of Dentistry, Seoul, Korea. [6]Institute for Innovation in Digital Healthcare, Yonsei University, Seoul, Korea. ✉email: jungcha@yuhs.ac

in the literature include E-guard (Envision TEC, Rock Hill, SC, USA), Dental LT Clear Resin (Formlabs Inc., Somerville, MA, USA) and Tera Harz TC-85 (Graphy Inc., Seoul, Korea)[13,14].

Among these resins, TC-85 is a photopolymer resin approved for medical device applications and has been adopted for the direct 3D printing of CAs[15]. It demonstrates viscous and flexible properties that may sustain force delivery during orthodontic movement[16,17]. Additionally, it exhibits shape memory behavior that may improve adaptability to tooth morphology, including undercuts, potentially enhancing contact with tooth surfaces[18]. Studies have also shown that it maintains microhardness comparable to thermoformed materials[19].

The biomechanics of CAs in orthodontics differ fundamentally from conventional bracket-based systems because force delivery depends on direct contact between the appliance and tooth surface. Force transmission can be reduced by aligner–tooth gaps and periodontal ligament flexibility, which allows roughly 0.04 mm of tooth displacement before initiating the biochemical response associated with tooth movement[20]. Therefore, a close fit between the tooth surface and the aligner, combined with material resilience, is critical for efficient force delivery [20,21].

Several research approaches have been proposed to evaluate CA fit or accuracy. Prior studies used scanning electron microscopy (SEM) to assess passive fit of commercial products, such as Invisalign and CA-Clear Aligner[21]. Other studies have compared the dimensional accuracy of thermoformed and 3D-printed CAs using scanning and superimposition techniques at specific tooth landmarks[22,23]. However, SEM requires destructive sectioning of samples, whereas scanning-based approaches require a surface spray that may compromise accuracy. To overcome these limitations, micro-computed tomography (micro-CT) has been suggested as a non-invasive and precise alternative for evaluating aligner thickness and gap width without physical sectioning, enabling detailed assessment of the aligner-tooth interface[20,24,25].

Despite these advances, most prior studies evaluated retainers using passive-state models, which do not reflect the dynamics of active tooth movement. Activated models introduce mechanical stress and deformation, providing a more realistic assessment of material behavior under clinical conditions. Therefore, the present study aimed to evaluate the fit of CAs on activated tooth models by measuring gap width using non-invasive, high-resolution micro-CT. Controlled labial displacements of 0.3 and 0.5 mm were applied to the upper right central incisor to simulate clinically relevant movement and compare aligner adaptation among material groups.

This study tested the following null hypotheses regarding activation levels in single tooth movement: (1) the fit of 3D-printed and thermoformed CAs would not differ significantly among tooth positions; (2) within each material group, the fit on tooth surfaces would not differ significantly between target and adjacent teeth. This study's findings are expected to improve clinical predictability in orthodontic treatment using CAs.

Results

Intrarater reliability for micro-CT gap width measurements was excellent, with an ICC value of 0.987 (95% CI 0.984–0.989).

Comparison of overall gap width for 3D-printed and thermoformed CAs by activation amount

The 3DP group showed the largest median gap width across all activation levels compared with the TM and TS groups (both $p < 0.001$). Gap width did not differ significantly with activation in the 3DP group ($p = 0.350$), whereas in the TM and TS groups, it increased significantly with greater activation (both $p < 0.001$). The TS group had the smallest median gap width in the passive state ($p < 0.001$), whereas the TM group had the smallest median gap width at 0.5-mm activation ($p < 0.001$; Table 1).

Comparison of gap width for 3D-printed and thermoformed CAs by activation amount and tooth position

In the 3DP group, gap widths showed no significant differences across activation levels or among individual teeth (#11, #12, #21, #16, and #26). In contrast, TM and TS groups exhibited significant increases in median gap width for the target (#11) and adjacent teeth (#12 and #21) with higher activation ($p < 0.001$), whereas anchorage

Activation amount	Median (IQR) Mean ± SD			*p*-value	Post hoc
	3DP (n = 30)	TM (n = 30)	TS (n = 30)		
0.0	0.059 (0.037–0.105) 0.077 ± 0.058	0.023 (0.000–0.047) 0.029 ± 0.028	0.012 (0.000–0.035) 0.020 ± 0.024	< 0.001***	3DP > TM > TS
0.3	0.070 (0.035–0.117) 0.091 ± 0.094	0.033 (0.012–0.089) 0.062 ± 0.076	0.023 (0.000–0.089) 0.058 ± 0.075	< 0.001***	3DP > TM, TS
0.5	0.071 (0.035–0.140) 0.098 ± 0.090	0.035 (0.012–0.150) 0.090 ± 0.112	0.042 (0.000–0.110) 0.088 ± 0.121	< 0.001***	3DP > TS > TM
p-value	0.350	< 0.001***	< 0.001***		
Post hoc	–	0.5 > 0.3 > 0.0	0.5, 0.3 > 0.0		

Table 1. Gap width (mm) of 3D-printed and thermoformed CAs by activation amount. Column-wise comparisons indicate differences among activation levels within each material, and row-wise comparisons indicate differences among materials within each activation level. Statistical analyses were performed using the Kruskal–Wallis test followed by post hoc Mann–Whitney U tests with Bonferroni correction. ***$p < 0.001$.

teeth (#16 and #26) showed no significant differences. At the passive state (P0.0), anterior teeth (#11, #12, and #21) had significantly larger gap widths compared with posterior anchorage teeth (#16 and #26) ($p < 0.001$). In both active states (A0.3 and A0.5), the largest gap widths were observed at #11 and #12 ($p < 0.001$).

As activation increased, gap width for #11 was significantly larger in the TM and TS groups than in the 3DP group (A0.3: $p = 0.010$; A0.5: $p < 0.001$). In contrast, gap widths for #12 and #21 did not differ significantly among the three groups in either active state. Additionally, #16 and #26 were unaffected by activation in all groups. Detailed values according to tooth position and material group are presented in Table 2.

Comparison of gap width by activation amount and measurement point in the anterior target segment within each material group

In the 3DP group, the buccal side of #12 ($p < 0.001$) and the palatal side of #11 ($p < 0.001$) showed the greatest gap width increases with activation. Conversely, the incisal edge of all three teeth (#11: $p = 0.006$; #12: $p = 0.019$; #21: $p = 0.025$) and the buccal side of #11 ($p = 0.008$) showed reduced gap width at 0.5-mm activation compared with the passive state. Variations for the 3DP group in the anterior target segment are shown in Supplementary Table S1, Figs. 1 and 4.

Tooth position	Activation amount	Median (IQR) Mean ± SD			*p*-value	Post hoc
		3DP (n = 30)	TM (n = 30)	TS (n = 30)		
Target (#11)	0.0	0.069 (0.048–0.089) 0.073 ± 0.035	0.048 (0.023–0.059) 0.047 ± 0.034	0.035 (0.0–0.052) 0.033 ± 0.030	< 0.001***	3DP > TM, TS
	0.3	0.076 (0.048–0.096) 0.076 ± 0.038	0.105 (0.047–0.248) 0.147 ± 0.115	0.158 (0.041–0.246) 0.148 ± 0.102	0.010*	TS, TM > 3DP
	0.5	0.055 (0.012–0.130) 0.079 ± 0.071	0.193 (0.068–0.376) 0.224 ± 0.159	0.233 (0.063–0.421) 0.237 ± 0.168	< 0.001**	TS, TM > 3DP
p-value		0.699	< 0.001***	< 0.001***		
Post hoc		–	0.5, 0.3 > 0.0	0.5 > 0.3 > 0.0		
Adjacent (#12)	0.0	0.067 (0.048–0.105) 0.076 ± 0.040	0.035 (0.023–0.058) 0.039 ± 0.026	0.023 (0.012–0.047) 0.028 ± 0.020	< 0.001***	3DP > TM, TS
	0.3	0.082 (0.042–0.151) 0.099 ± 0.063	0.117 (0.063–0.140) 0.100 ± 0.046	0.089 (0.059–0.125) 0.091 ± 0.041	0.629	–
	0.5	0.073 (0.048–0.175) 0.113 ± 0.092	0.163 (0.059–0.210) 0.138 ± 0.079	0.111 (0.071–0.193) 0.133 ± 0.071	0.146	–
p-value		0.283	< 0.001***	< 0.001***		
Post hoc		–	0.5 > 0.3 > 0.0	0.5 > 0.3 > 0.0		
Adjacent (#21)	0.0	0.059 (0.048–0.082) 0.067 ± 0.032	0.037 (0.012–0.059) 0.040 ± 0.031	0.023 (0.0–0.048) 0.030 ± 0.029	< 0.001***	3DP > TM > TS
	0.3	0.071 (0.048–0.096) 0.074 ± 0.035	0.061 (0.037–0.082) 0.059 ± 0.035	0.063 (0.023–0.089) 0.063 ± 0.049	0.182	–
	0.5	0.073 (0.042–0.094) 0.075 ± 0.046	0.078 (0.052–0.111) 0.085 ± 0.052	0.080 (0.063–0.107) 0.094 ± 0.070	0.431	–
p-value		0.518	< 0.001***	< 0.001***		
Post hoc		–	0.5 > 0.3 > 0.0	0.5, 0.3 > 0.0		
Anchorage (#16 & 26)	0.0	0.058 (0.023–0.125) 0.082 ± 0.078	0.012 (0.000–0.023) 0.012 ± 0.012	0.000 (0.000–0.012) 0.006 ± 0.009	< 0.001***	3DP > TM > TS
	0.3	0.050 (0.023–0.140) 0.101 ± 0.130	0.012 (0.000–0.020) 0.012 ± 0.012	0.0 (0.000–0.012) 0.005 ± 0.009	< 0.001***	3DP > TM > TS
	0.5	0.074 (0.023–0.189) 0.110 ± 0.107	0.012 (0.006–0.023) 0.015 ± 0.012	0.0 (0.000–0.012) 0.004 ± 0.007	< 0.001***	3DP > TM > TS
p-value		0.412	0.028*	0.063		
Post hoc		–	–	–		
***p*-value (Post hoc)**	0.0	0.504 –	< 0.001*** (#11, 12, 21 > #16 & 26)	< 0.001*** (#11, 12, 21 > #16 & 26)		
	0.3	0.140 –	< 0.001*** (#11, 12 > #21 > #16 & 26)	< 0.001*** (#11, 12 > #21 > #16 & 26)		
	0.5	0.259 –	< 0.001*** (#11, 12 > #21 > #16 & 26)	< 0.001*** (#11, 12 > #21 > #16 & 26)		

Table 2. Gap width (mm) of 3D-printed and thermoformed CAs by activation amount and tooth position. Column-wise comparisons indicate differences for a given material: (i) among activation levels within each tooth position and (ii) among tooth positions within each activation level. Row-wise comparisons indicate differences among materials within each activation level. Statistical analyses were performed using the Kruskal–Wallis test followed by post hoc Mann–Whitney U tests with Bonferroni correction. *$p < 0.05$; ***$p < 0.001$.

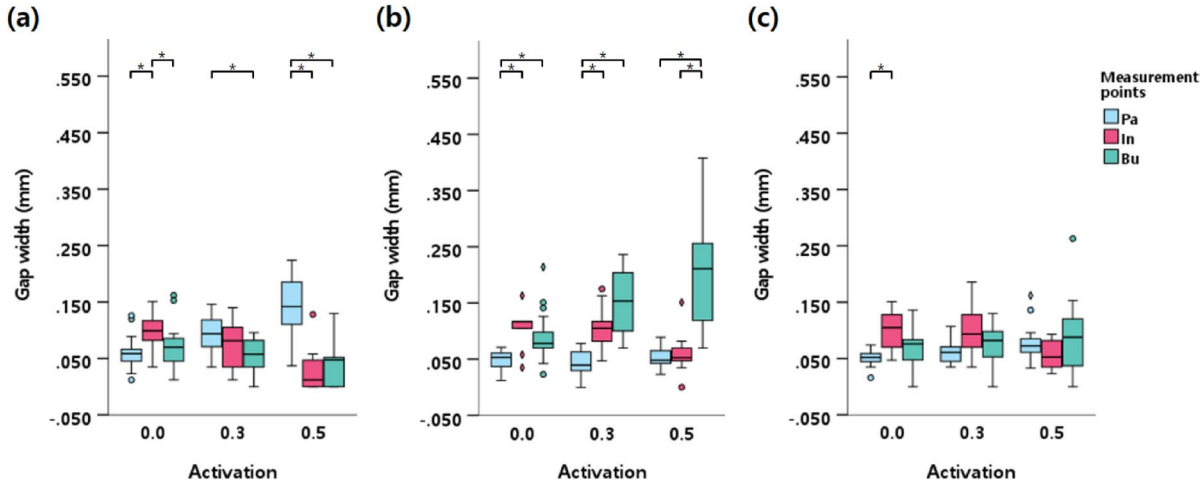

Fig. 1. Median (IQR) gap width of 3DP group by activation amount and measurement point in the anterior target segment. (**a**) Target tooth #11, (**b**) adjacent tooth #12, and (**c**) adjacent tooth #21. Outliers (> 1.5 × IQR) are shown by closed circles, and extreme outliers (> 3 × IQR) by diamonds. Asterisks indicate statistically significant post hoc differences after Bonferroni correction ($p < 0.017$). *Pa* (palatal): *Pm* (palatal midpoint) + *Pg* (palatogingival point); *In* (incisal): *In/Oc* (incisal or occlusal point); *Bu* (buccal): *Bm* (buccal midpoint) + *Bg* (buccogingival point). Complete data and statistical results are provided in Supplementary Table S1.

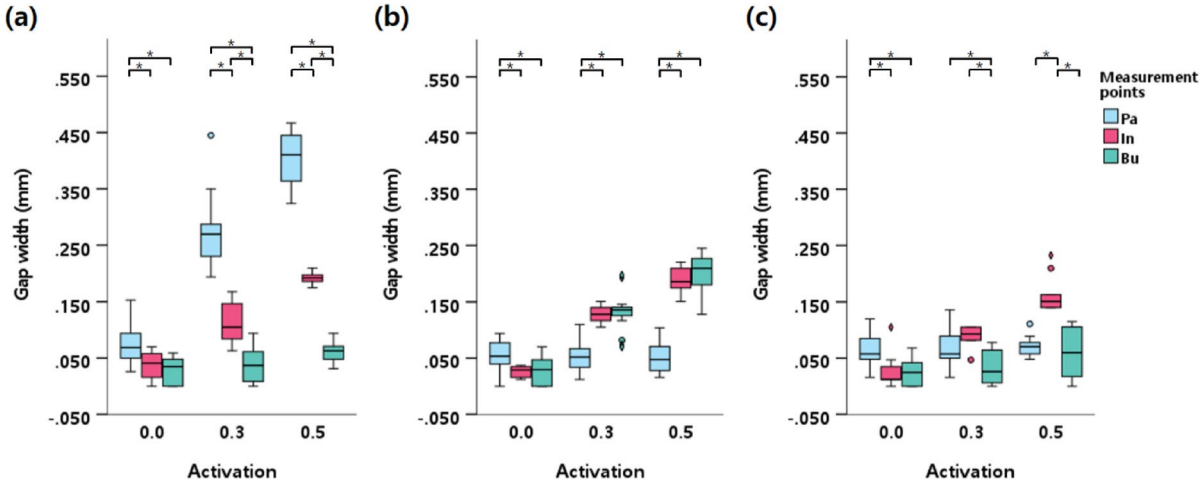

Fig. 2. Median (IQR) gap width of TM group by activation amount and measurement point in the anterior target segment. (**a**) Target tooth #11, (**b**) adjacent tooth #12, and (**c**) adjacent tooth #21. Outliers (> 1.5 × IQR) are shown by closed circles, and extreme outliers (> 3 × IQR) by diamonds. Asterisks indicate statistically significant post hoc differences after Bonferroni correction ($p < 0.017$). Abbreviations as in Fig. 1. Complete data and statistical results are provided in Supplementary Table S2.

In the TM group, the palatal side of #11 ($p < 0.001$) and the buccal side of #12 ($p < 0.001$) showed the largest gap width increases. The incisal edge of all three teeth (#11: $p < 0.001$; #12: $p < 0.001$; #21: $p < 0.001$) also increased significantly with activation, whereas the palatal sides of #12 and #21 showed no significant change. Variations for the TM group are presented in Supplementary Table S2, Figs. 2 and 4.

In the TS group, the palatal side of #11 ($p < 0.001$) and the incisal edge of all three teeth (#11: $p < 0.001$; #12: $p < 0.001$; #21: $p < 0.001$) exhibited the largest increases in gap width with activation. Median gap widths at all surfaces of all three teeth increased significantly with activation level. Variations for the TS group are summarized in Supplementary Table S3, Figs. 3. and 4.

Discussion

In CA therapy, the gap width of CAs is a key factor that strongly influences orthodontic treatment, and the inner surface of the aligner should remain as close to the teeth as possible to apply clinically effective forces[20,26,27]. This study compared the fit of 3D-printed and thermoformed CAs using micro-CT under passive and activated tooth models, aiming to clarify how material and activation affect aligner adaptation. The results demonstrated that (1)

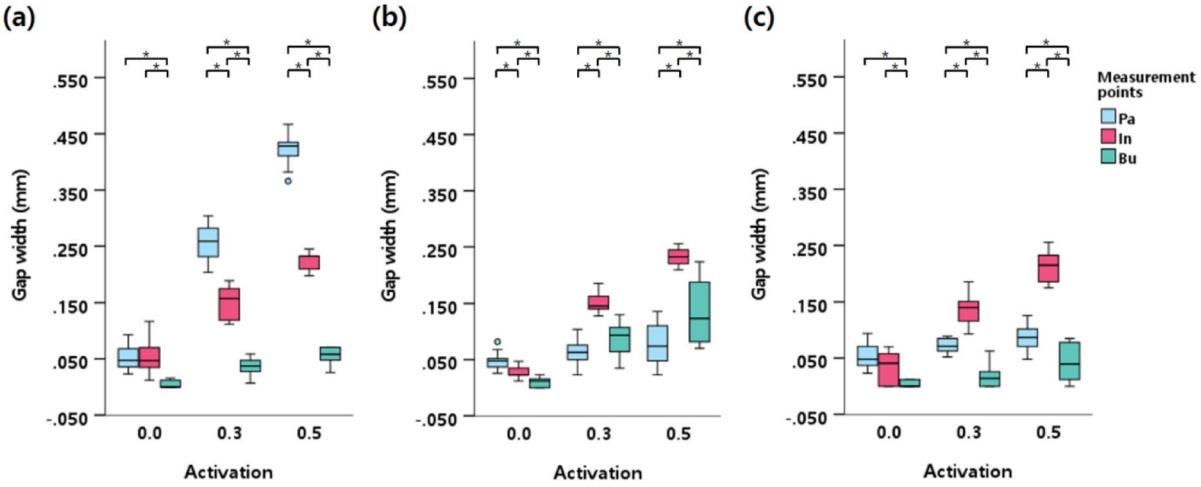

Fig. 3. Median (IQR) gap width of TS group by activation amount and measurement point in the anterior target segment. (**a**) Target tooth #11, (**b**) adjacent tooth #12, and (**c**) adjacent tooth #21. Outliers (> 1.5 × IQR) are shown by closed circles, and extreme outliers (> 3 × IQR) by diamonds. Asterisks indicate statistically significant post hoc differences after Bonferroni correction ($p < 0.017$). Abbreviations as in Fig. 1. Complete data and statistical results are provided in Supplementary Table S3.

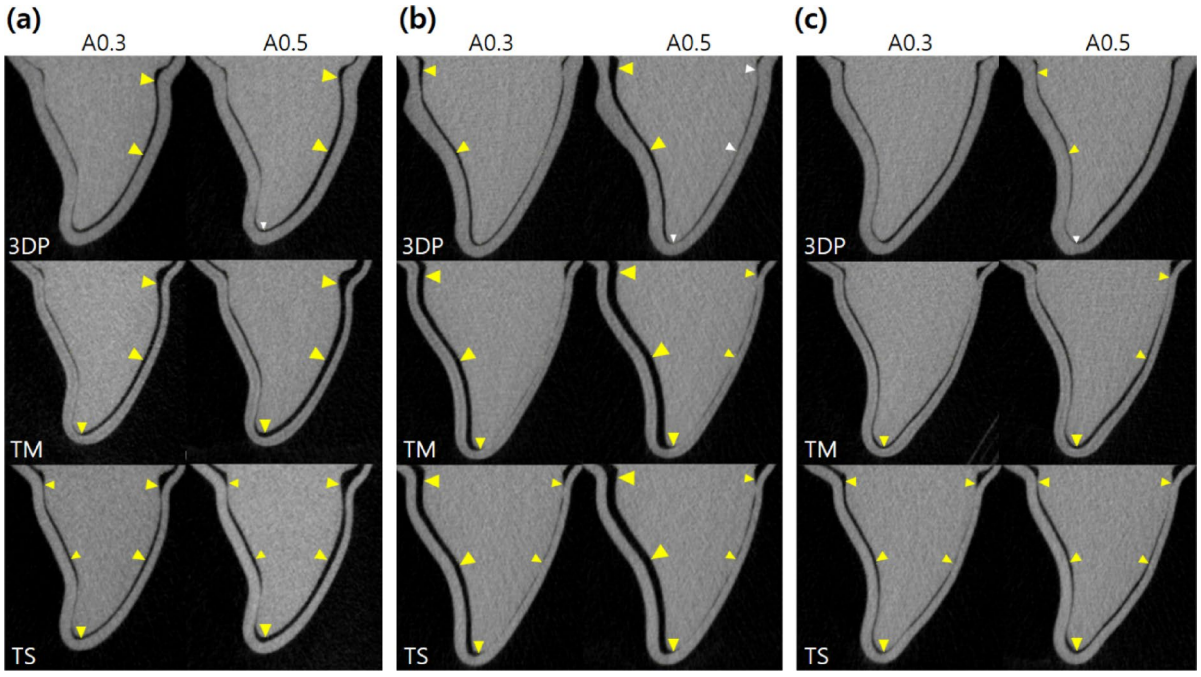

Fig. 4. Representative sagittal micro-CT images showing the gap width between the aligner material group and the tooth surface at 0.3-mm activation (A0.3) and 0.5-mm activation (A0.5). The yellow and white arrows indicate significant increases and decreases in gap width, respectively, with greater activation. (**a**) Adjacent tooth #12, (**b**) target tooth #11, and (**c**) adjacent tooth #21.

the fit of 3D-printed and thermoformed CAs differed significantly among tooth positions, with material-specific responses to activation level and (2) within each material group, the fit on the tooth surfaces differed significantly between target and adjacent teeth under activation, leading to rejection of both null hypotheses at a significance level of $\alpha = 0.05$.

Micro-CT was selected because it enables non-invasive, high-resolution evaluation of the aligner–tooth interface while allowing standardized sectioning at identical locations across specimens. This approach is particularly suitable for activated models, where material behavior under activation can be assessed without compromising specimen integrity. Nevertheless, despite the use of standardized section definitions and predefined landmarks, complete standardization of measurement point selection remains challenging due to the

complexity of tooth morphology, which may contribute to minor but acceptable measurement variability within the resolution limits of the technique.

Significant differences in gap width were observed among the three material groups depending on activation level. The 3DP group consistently exhibited significantly larger median gap widths (0.059–0.071 mm) compared with the TM (0.023–0.035 mm) and TS (0.012–0.042 mm) groups at all activation levels (P0.0, A0.3, and A0.5), indicating lower overall fit. Differences in overall fit at the P0.0 state among groups align with prior passive-state studies, which reported that 3D-printed CAs showed greater gap widths relative to thermoformed CAs, with no significant differences observed between the TM and TS group[25]. Cole et al. similarly found that 3D-printed retainers had the greatest deviation from original reference models, whereas vacuum-formed retainers had the least[22]. Accumulated polymerization shrinkage during printing has been associated with the broadly lower fit of 3D-printed CAs[28].

Notably, despite the 3DP group consistently showing larger gap widths, it was unaffected by increases in activation, suggesting that the direct-printed material maintains dimensional stability under stress. This contrasts with thermoformed materials, where greater activation induced deformation. The thermomechanical and viscoelastic properties of the TC-85 resin material likely contributed to its distinct behavior. According to Lee et al., TC-85 exhibited rapid stress relaxation at 37 °C, with residual force decreasing from 18.0 to 1.0 N after 13 cycles[16]. This property may have allowed the aligner to adapt more gradually and uniformly to the activated dentition, thereby reducing localized stress at the target site. Furthermore, the higher loss tangent of TC-85 (0.16) compared with PETG (0.004) at 37 °C indicates its greater viscous behavior under thermal conditions[16]. This elevated viscosity and lower elastic modulus in TC-85 resin likely contributed to enhanced creep compliance and stress relaxation[17], enabling smooth deformation of the material and allowing more gradual adaptation to misaligned dentition without disengagement.

For effective tooth movement with conventional thermoplastic CAs, it is recommended to move teeth by 0.25–0.33 mm per step[29]. Gao et al. suggested that the ideal aligner activation increment should be 0.20–0.50 mm[30,31]. Therefore, we tested activation at 0.3 and 0.5 mm, representing the average and upper end of the recommended activation range for thermoformed aligners, respectively. Although the initial gap width of the 3DP group was larger than that of the thermoformed groups, minimal degradation of fit occurred during tooth movement, particularly at 0.5-mm activation, owing to the higher flexibility and broader elastic range of CAs made with TC-85[16]. This suggests that aligner deformation is less pronounced with greater activation, indicating potential for more tooth movement per step, which may reduce the number of treatment steps or shorten treatment duration. However, force transfer efficiency may still be affected by lower initial fit; therefore, further validation is needed to confirm whether fit stability translates into efficient clinical performance.

The TS and TM groups showed the smallest gap widths in the P0.0 and A0.5 states, respectively. This pattern can be explained by the multi-layer composition of TM materials, which include elastic media between outer layers that may enhance resistance to deformation under high stress[11]. In contrast, single-layer materials, although initially stiffer owing to a higher elastic modulus, have been shown to lose mechanical stability after repeated stress or simulated aging[32], potentially leading to greater gap widening at higher activation levels.

Fit patterns across teeth varied with activation level and material group. For intertooth comparisons, the 3DP group maintained relatively uniform fit across target (#11), adjacent (#12 and #21), and anchorage (#16 and #26) teeth, regardless of activation. In contrast, the TM and TS groups showed significantly lower fit in target (#11) and adjacent (#12 and #21) teeth with increasing activation, whereas anchorage teeth (#16 and #26) showed no significant change at any activation level. Additionally, at A0.3 and A0.5 states, target #11 and adjacent #12 demonstrated larger gap widths compared with adjacent #21 in both thermoformed groups. The lower fit of #12 relative to #21 at active states may be explained by morphological differences, such as shorter crowns, and the mechanical properties of thermoformed materials[7,33].

The fit of tooth surfaces in the anterior target segment under activation was material-dependent, and the degree of displacement affected not only the target but also the adjacent teeth. For the 3DP group, the palatal side of #11 (0.059–0.142 mm) and buccal side of #12 (0.078–0.211 mm) responded most to activation. However, the buccal side of #11 and incisal edges of all three teeth showed a significant reduction in gap width at 0.5-mm activation, a pattern distinct from that of the thermoplastic groups. TC-85 resin provides greater surface resilience through its thermomechanical and viscoelastic properties[16,17], maintaining structural conformity and promoting adaptation in target and adjacent teeth even during activation, particularly at movement sites. In contrast, the palatal side of #11 showed the greatest increases in gap width (TM: 0.069–0.411 mm; TS: 0.048–0.429 mm), highlighting challenges in adaptation at the movement-facing side in the TM and TS groups. PETG and similar thermoformed materials, characterized by higher elasticity and lower viscosity[16], likely generated tension from adjacent contact zones, causing dislodgement between the tooth model and aligner.

In clinical situations requiring multiple-tooth movement, the fit characteristics of aligner materials must be considered. During lingual movement of the central incisor, a gap forms at the labial surface of the adjacent lateral incisor; if lateral incisor rotation is also required, this gap may impair movement. In cases involving both lingual movement and intrusion, conventional thermoplastic appliances may be less effective for intrusion because of reduced fit at the incisal edge. Bodily tooth movement often coincides with tipping, and although CAs are effective for leveling and alignment, they face difficulties with movements such as extrusion, rotation, and torque control, which remain unpredictable[34]. CAs often induce uncontrolled tipping and relative intrusion, concentrating force on the incisal edge or occlusal surface, especially when intimate fit and full surface contact are lacking[26,35,36]. Reduced fit can also lift aligners during torque-related root movement, complicating generation of effective couple force[26]. To compensate, overengineering with additional preset torque and counter-moments should be considered[37–39]. Attachments serve as important auxiliary elements of CA therapy[40,41], and stepwise tooth movement or reduced displacement per step is often necessary. From a design perspective, digital workflows with 3D-printed materials can support more precise planning of complex tooth movements.

The present study should be interpreted within several limitations. First, experimental constraints prevented simulation of an oral environment at 37 ℃ with high relative humidity during micro-CT scanning, which may have affected fit. Second, as an in vitro investigation, this study was limited to static assessment of aligner fit during labiolingual displacement of a single tooth. Other types of tooth movements, such as rotations and multidimensional displacements involving multiple teeth, as well as actual tooth movement patterns and clinical efficacy, were not evaluated. Third, the aligners were not exposed to intraoral degradation factors, including salivary enzymes, pH fluctuations, masticatory forces, or aging conditions, that affect material properties during clinical use. Accordingly, this study focused on initial fit assessment and did not evaluate long-term material behavior or dynamic changes during wear. Further research is needed to determine whether the observed material-dependent fit behaviors under activation translate to differences in force delivery and treatment outcomes in clinical practice.

Conclusion

The fit of CAs differed between 3D-printed and thermoformed materials under activation. 3D-printed CAs exhibited greater overall gap widths than thermoformed CAs, and their gap widths were not significantly affected by increasing activation. In contrast, thermoformed CAs showed significant activation-dependent increases in gap width, particularly at the target and adjacent teeth. All material groups exhibited significant surface-specific fit variations at target and adjacent teeth, with thermoformed CAs showing greater increases relative to 3D-printed CAs. These findings indicate that both manufacturing technique and prescribed activation influence aligner fit under static laboratory conditions.

Methods

Sample preparation

Three types of tooth evaluation model were created: passive-state (P0.0), 0.3-mm active-state (A0.3), and 0.5-mm active-state (A0.5). For the P0.0 model, a standardized upper dental arch model from Korean adults with normal occlusion (CON2001-UL-SP-FEM-32, Nissin Dental, Kyoto, Japan) was scanned with an intraoral scanner (D250, 3Shape, Copenhagen, Denmark) to generate an STL file. Using this file, the A0.3 and A0.5 models were produced by moving the upper right central incisor (#11: target tooth) bodily towards the labial direction by 0.3 and 0.5 mm, respectively, using CAD/CAM software (3Shape Ortho System, Copenhagen, Denmark). Digital models (60 × 50 × 20 mm; S-100, Graphy Inc., Seoul, Korea) were printed at 30 units per model type (total n = 90) using a DLP 3D printer (ASIGA Pro 4 K 385, Asiga, Alexandria, Australia). After printing, the models were removed from the build platform and cleaned with 99.5% isopropyl alcohol (IPA) for 1 min using two fresh baths (30 s each). If residual resin was observed, gentle brushing was performed followed by an additional IPA rinse. Residual IPA was removed using compressed air, and post-curing was performed using the Tera Harz Cure (Graphy Inc., Seoul, Korea) under level 1 for 5 min. To minimize potential dimensional changes, printed models were stored at room temperature in a light-shielded environment, and aligner fitting was completed within 3 days after model fabrication prior to micro-CT acquisition.

Thirty thermoformed CA samples were fabricated per group. Thermoformed CAs were divided into two groups: the multi-layer (TM) group, with copolyester outer shells and thermoplastic elastomer inner shells (CA pro, Scheu-Dental, Iserlohn, Germany), and the single-layer (TS) group, with a PETG sheet (Duran, Scheu-Dental, Iserlohn, Germany). A 0.75-mm-thick thermoplastic material was vacuum-thermoformed on a passive-state model using a thermomolding caster (Ministar, Scheu-Dental, Iserlohn, Germany) under manufacturer-recommended thermal deformation conditions. To maintain consistency, the model base was prepared to a uniform height[42], and its position was standardized on the platform. After thermoforming, CAs were separated from the model, and the gingival line of the aligner was trimmed straight, 2 mm beneath the gingival margin.

Thirty 3D-printed CA samples were prepared using photo-polymerizable polyurethane resin (TC-85, Graphy Inc., Seoul, Korea). Based on the passive-state STL file, CAs were designed using CAD software (Direct Aligner Designer, Graphy Inc., Seoul, Korea) at 0.5-mm thickness, 50-μm offset from tooth surfaces, and 0-μm offset from the gingiva. Printing was performed with a DLP 3D printer (ASIGA UV MAX 385, Asiga, Alexandria, Australia) at 50-μm layer thickness. CAs were printed with a 20° orientation and minimal strut supports. This orientation was chosen to reduce support-contact artifacts on the fitting surface and to improve printing stability by minimizing suction-related deformation during layer-by-layer fabrication. This printing strategy was adopted to preserve dimensional fidelity of the intaglio surface, which is critical for accurate evaluation of aligner fit. Uncured resin was removed via centrifugation for 5 min using the Tera Harz spinner (Graphy Inc., Seoul, Korea), after which samples were cured using the Tera Harz Cure (Graphy Inc., Seoul, Korea) for 20 min under level 2 nitrogen conditions with ultraviolet light (385–405 nm). This inert curing prevented oxygen inhibition and improved material properties. Final cleaning was performed using flowing water and ultrasonic cleaning for 2 min at 80 ℃. CAs were boiled for 1 min at 100 ℃ and dried for 10 min. Figure 5 illustrates the experimental design and study workflow.

Gap width measurement using micro-CT

The micro-CT acquisition and measurement protocol followed prior methodology[25]. CAs were applied to their respective evaluation models (P0.0, A0.3, and A0.5). The 3D-printed CAs were conditioned in warm water (80 ℃), following the manufacturer's guidelines, whereas thermoformed CAs were immediately inserted at room temperature. Subsequently, 3D-printed samples were dried at 37 ℃ to restore their original configuration and structural integrity. All aligners (n = 10 per condition) were scanned using a high-resolution micro-CT device (Skyscan1173, Bruker, Billerica, MA, USA) at 40 kV, 200 μ A, and 34.9 μm of resolution, yielding 90 scans in total.

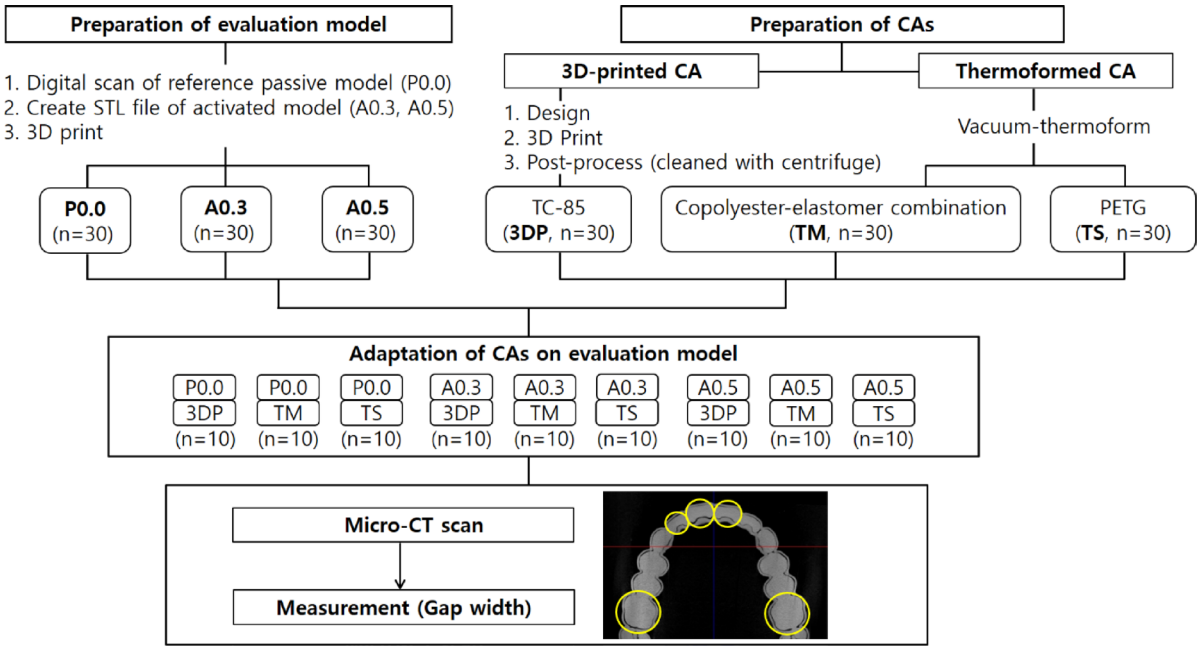

Fig. 5. Flowchart of the experimental design and process.

The upper right central incisor (#11: target), right lateral incisor (#12: adjacent), left central incisor (#21: adjacent), and first molars (#16 and #26: anchorage) were re-orientated using Dataviewer software (version 1.5.6.2, Bruker, MA, USA). Slices were obtained using the model base as the horizontal reference plane. For each evaluated tooth, a volume of interest (VOI) of identical size was defined to include the most mesial and distal contact points, and a reference line connecting these two points was constructed. The sectional plane was set perpendicular to this mesiodistal reference line and passing through its midpoint, thereby generating a reproducible sagittal section for each tooth (Fig. 6). The standardized sagittal cross-sectional images were saved and analyzed using CTAn software (version 1.17.7.1, Bruker, MA, USA) at 300× magnification (Fig. 6).

Gap width was measured as the shortest perpendicular distance from the inner surface of the aligner to the tooth surface at predefined reference points on the selected section. Reference points included buccal and palatal gingival margins, buccal and palatal midpoints (defined as the midpoint between the gingival margin and the incisal/occlusal point), and incisal/occlusal points (incisal edge and occlusal cusp tips) (Fig. 6)[24]. The occlusal points of posterior teeth included buccal and palatal cusp tips, considered clinically as a single plane; thus, rather than analyzing their measurement values separately (*Oc1* and *Oc2*), we interpreted them using mean values.

For statistical analysis of the anterior target segment (#11, #12, and #21), five measurement points were grouped into three anatomical regions: buccal, incisal, and palatal. The buccal (*Bu*) measurement was considered the combined buccogingival margins (*Bg*) and buccal midpoints (*Bm*) values, whereas the palatal (*Pa*) measurement was defined as the combined palatogingival margins (*Pg*) and palatal midpoints (*Pm*) values, representing the overall buccal and palatal regions of the teeth, respectively. In total, 2,430 measurement points were assessed by a single examiner and remeasured after a 2-week interval to evaluate intrarater reproducibility. The intraclass correlation coefficient (ICC) was calculated using a two-way mixed-effects model with absolute agreement (ICC(3,1)) for repeated measurements.

Statistical analysis

Data were analyzed using SPSS software (version 28.0, IBM Corp., Armonk, NY, USA). The normality of data distribution was assessed using the Shapiro–Wilk test, which indicated non-normality. Median gap widths of aligners were compared by tooth position and measurement point across activation levels using the nonparametric Kruskal–Wallis test for multiple comparisons, followed by the post hoc Mann–Whitney U test with Bonferroni correction. The significance level ($\alpha = 0.05$) was adjusted according to the number of statistical tests performed ($p < 0.017$ for three-group comparisons and $p < 0.0125$ for four-group comparisons).

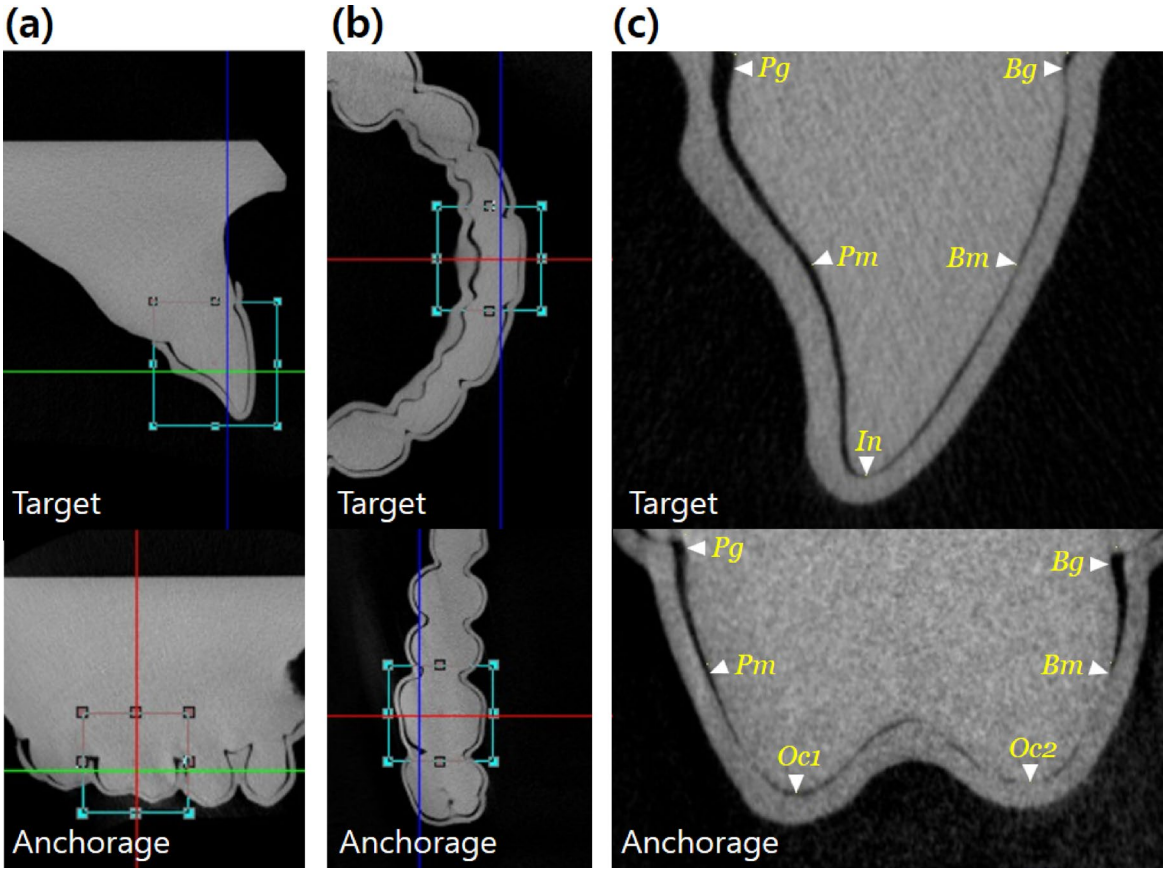

Fig. 6. Micro-CT analysis of gap widths in an individual tooth. (**a**) Slices of the focused tooth obtained from micro-CT imaging using a horizontal plane from the model base, and (**b**) perpendicular to the line connecting the most mesial and distal contact points of the tooth, with VOI (blue box) applied in Dataviewer. (**c**) Measurement of gap width using CTAn. White arrows indicate measurement points: *Pg,* palatogingival; *Pm,* palatal midpoint; *In/Oc*, incisal or occlusal; *Bm,* buccal midpoints; *Bg,* buccogingival.

Data availability

All data that support the findings of this study are available from the corresponding author upon reasonable request.

Received: 20 November 2025; Accepted: 28 January 2026
Published online: 09 February 2026

References

1. Macrì, M., Murmura, G., Varvara, G., Traini, T. & Festa, F. Clinical performances and biological features of clear aligners materials in orthodontics. *Front. Mater.* **9**, 819121. https://doi.org/10.3389/fmats.2022.819121 (2022).
2. Lynch, N. M. et al. Clear aligner therapy in the mixed dentition: Indications and practitioner perspectives. *Am. J. Orthod. Dentofac. Orthop.* **164**, 172–182 (2023).
3. Weir, T. Clear aligners in orthodontic treatment. *Aust. Dent. J.* **62**(Suppl 1), 58–62 (2017).
4. Tamburrino, F. et al. Mechanical properties of thermoplastic polymers for aligner manufacturing: In vitro study. *Dent. J. (Basel)* **8**, 47. https://doi.org/10.3390/dj8020047 (2020).
5. Liu, J. & Cha, J.-Y. Mechanical and biological properties of current materials of clear aligner. *J. Korean Dent. Assoc.* **62**, 302–316 (2024).
6. Zhang, N., Bai, Y., Ding, X. & Zhang, Y. Preparation and characterization of thermoplastic materials for invisible orthodontics. *Dent. Mater. J.* **30**, 954–959 (2011).
7. Dupaix, R. B. & Boyce, M. C. Finite strain behavior of poly (ethylene terephthalate) (PET) and poly (ethylene terephthalate)-glycol (PETG). *Polymer (Guildf)* **46**, 4827–4838 (2005).
8. Frick, A. & Rochman, A. Characterization of TPU-elastomers by thermal analysis (DSC). *Polym. Test.* **23**, 413–417 (2004).
9. Lu, Q.-W. & Macosko, C. W. Comparing the compatibility of various functionalized polypropylenes with thermoplastic polyurethane (TPU). *Polymer (Guildf)* **45**, 1981–1991 (2004).
10. Jindal, P., Juneja, M., Siena, F. L., Bajaj, D. & Breedon, P. Mechanical and geometric properties of thermoformed and 3D printed clear dental aligners. *Am. J. Orthod. Dentofac. Orthop.* **156**, 694–701 (2019).
11. Ahn, H. W., Kim, K. A. & Kim, S. H. A new type of clear orthodontic retainer incorporating multi-layer hybrid materials. *Korean J. Orthod.* **45**, 268–272 (2015).
12. Bichu, Y. M. et al. Advances in orthodontic clear aligner materials. *Bioact. Mater.* **22**, 384–403 (2023).
13. Boo, H. S., Sivarajan, S., Nor zahidah Mohd Tahir, N. & Bahar, A. D. Accuracy of three-dimensionally printed retainers and aligners: a systematic review. *J. Orofac. Orthop.* https://doi.org/10.1007/s00056-024-00570-x (2025).

14. Dantagnan, C.-A. et al. Biocompatibility of direct printed clear aligners: a systematic review of in vitro studies. *J. Int. Orthod.* **23**, 101028. https://doi.org/10.1016/j.ortho.2025.101028 (2025).
15. Rajasekaran, A. & Chaudhari, P. K. Integrated manufacturing of direct 3D-printed clear aligners. *Front. Dent. Med.* **3**, 1089627. https://doi.org/10.3389/fdmed.2022.1089627 (2023).
16. Lee, S. Y. et al. Thermo-mechanical properties of 3D printed photocurable shape memory resin for clear aligners. *Sci. Rep.* **12**, 6246. https://doi.org/10.1038/s41598-022-09831-4 (2022).
17. Choi, J. Y. et al. Mechanical and viscoelastic properties of a temperature-responsive photocurable resin for 3D printed orthodontic clear aligners. *Sci. Rep.* **15**, 23530. https://doi.org/10.1038/s41598-025-93026-0 (2025).
18. Kim, D. W. et al. Force and moment analysis of clear aligners: impact of material properties and design on premolar rotation. *Korean J. Orthod.* **55**, 212–223 (2025).
19. Atta, I. et al. Physiochemical and mechanical characterisation of orthodontic 3D printed aligner material made of shape memory polymers (4D aligner material). *J. Mech. Behav. Biomed. Mater.* **150**, 106337. https://doi.org/10.1016/j.jmbbm.2023.106337 (2024).
20. Lombardo, L. et al. MicroCT X-ray comparison of aligner gap and thickness of six brands of aligners: an in-vitro study. *Prog. Orthod.* **21**, 12. https://doi.org/10.1186/s40510-020-00312-w (2020).
21. Mantovani, E. et al. Scanning electron microscopy evaluation of aligner fit on teeth. *Angle Orthod.* **88**, 596–601 (2018).
22. Cole, D., Bencharit, S., Carrico, C. K., Arias, A. & Tüfekçi, E. Evaluation of fit for 3D-printed retainers compared with thermoform retainers. *Am. J. Orthod. Dentofac. Orthop.* **155**, 592–599 (2019).
23. Koenig, N. et al. Comparison of dimensional accuracy between direct-printed and thermoformed aligners. *Korean J. Orthod.* **52**, 249–257 (2022).
24. Palone, M. et al. Micro-computed tomography evaluation of general trends in aligner thickness and gap width after thermoforming procedures involving six commercial clear aligners: An in vitro study. *Korean J. Orthod.* **51**, 135–141 (2021).
25. Park, S. Y. et al. Comparison of translucency, thickness, and gap width of thermoformed and 3D-printed clear aligners using micro-CT and spectrophotometer. *Sci. Rep.* **13**, 10921. https://doi.org/10.1038/s41598-023-36851-5 (2023).
26. Hahn, W. et al. Torquing an upper central incisor with aligners—acting forces and biomechanical principles. *Eur. J. Orthod.* **32**, 607–613 (2010).
27. Barone, S., Paoli, A., Razionale, A. V. & Savignano, R. Computational design and engineering of polymeric orthodontic aligners. *Int. J. Numer. Method Biomed. Eng.* **33**, e2839. https://doi.org/10.1002/cnm.2839 (2017).
28. Yang, M.-S., Kim, S.-K., Heo, S.-J., Koak, J.-Y. & Park, J.-M. Investigation of the marginal fit of a 3D-printed three-unit resin prosthesis with different build orientations and layer thicknesses. *J. Adv. Prosthodont.* **14**, 250–261 (2022).
29. Kravitz, N. D., Kusnoto, B., BeGole, E., Obrez, A. & Agran, B. How well does Invisalign work? A prospective clinical study evaluating the efficacy of tooth movement with Invisalign. *Am. J. Orthod. Dentofac. Orthop.* **135**, 27–35 (2009).
30. Gao, L. & Wichelhaus, A. Forces and moments delivered by the PET-G aligner to a maxillary central incisor for palatal tipping and intrusion. *Angle Orthod.* **87**, 534–541 (2017).
31. Grant, J. et al. Forces and moments generated by 3D direct printed clear aligners of varying labial and lingual thicknesses during lingual movement of maxillary central incisor: An in vitro study. *Prog. Orthod.* **24**, 23. https://doi.org/10.1186/s40510-023-00475-2 (2023).
32. Šimunović, L., Jurela, A., Sudarević, K., Bačić, I. & Meštrović, S. Differential stability of one-layer and three-layer orthodontic aligner blends under thermocycling: Implications for clinical durability. *Acta Stomatol. Croat.* **57**, 286–299 (2023).
33. Shirey, N., Mendonca, G., Groth, C. & Kim-Berman, H. Comparison of mechanical properties of 3-dimensional printed and thermoformed orthodontic aligners. *Am. J. Orthod. Dentofac. Orthop.* **163**, 720–728 (2023).
34. Rossini, G., Parrini, S., Castroflorio, T., Deregibus, A. & Debernardi, C. L. Efficacy of clear aligners in controlling orthodontic tooth movement: a systematic review. *Angle Orthod.* **85**, 881–889 (2015).
35. Simon, M., Keilig, L., Schwarze, J., Jung, B. A. & Bourauel, C. Forces and moments generated by removable thermoplastic aligners: Incisor torque, premolar derotation, and molar distalization. *Am. J. Orthod. Dentofac. Orthop.* **145**, 728–736 (2014).
36. Brezniak, N. The clear plastic appliance: A biomechanical point of view. *Angle Orthod.* **78**, 381–382 (2008).
37. Sim, D. & Farella, M. Methodological issues in current clear aligner research. *Semin. Orthod.* https://doi.org/10.1053/j.sodo.2025.02.005 (2025).
38. Kim, K., Choi, Y.-K., Kim, S.-H., Kim, S.-S. & Kim, Y.-I. Multi-step finite element simulation for clear aligner space closure: a proof-of-concept compensation protocol. *Sci. Rep.* **15**, 22220. https://doi.org/10.1038/s41598-025-07110-6 (2025).
39. Niu, C. et al. Prospects for 3D-printing of clear aligners—A narrative review. *Front. Mater.* **11**, 1438660. https://doi.org/10.3389/fmats.2024.1438660 (2024).
40. Nucera, R. et al. Effects of composite attachments on orthodontic clear aligners therapy: a systematic review. *Materials (Basel)* **15**, 533. https://doi.org/10.3390/ma15020533 (2022).
41. Jedliński, M. et al. Attachments for the orthodontic aligner treatment—State of the art—A comprehensive systematic review. *Int. J. Environ. Res. Public Health* **20**, 4481. https://doi.org/10.3390/ijerph20054481 (2023).
42. Ihssen, B. A., Kerberger, R., Rauch, N., Drescher, D. & Becker, K. Impact of dental model height on thermoformed PET-G aligner thickness—an in vitro micro-CT study. *Appl. Sci.* **11**, 6674. https://doi.org/10.3390/app11156674 (2021).

Author contributions

S.Y.L. and J.Y.C. designed the experiments and analyzed the data. S.Y.L. performed all the experiments and wrote the manuscript. S.H.C., H.S.Y., S.H.P., J.S.K., S.J.K., J.L. and J.Y.C. provided manuscript writing assistance and critically revised the manuscript for important intellectual content. All authors reviewed and approved the final manuscript.

Funding

This work was supported by the Korea Medical Device Development Fund grant funded by the Korea government (the Ministry of Science and ICT, the Ministry of Trade, Industry and Energy, the Ministry of Health & Welfare, the Ministry of Food and Drug Safety) (Project Number: 1475013501, RS-2023-00208725).

Declarations

Competing interests

The authors declare no competing interests.

Additional information

Supplementary Information The online version contains supplementary material available at https://doi.org/10.1038/s41598-026-37964-3.

Correspondence and requests for materials should be addressed to J.-Y.C.